Papers

Volume 8: 2008-2014

Thoft-Christensen, Palle

Publication date:
2014

Document Version
Publisher's PDF, also known as Version of record

CHAPTER 140

DETERIORATION OF REINFORCED CONCRETE STRUCTURES[1]

P. Thoft-Christensen
Aalborg University, Aalborg, Denmark

1. INTRODUCTION

Modelling of deterioration of reinforced concrete structures is usually based on observations of the deterioration of existing structures and on comprehensive experiments in laboratories. By such observations the so-called deterioration profile (deterioration, reliability, or capacity as a function of time) may be estimated. In the past a large number of such observation based profiles have been estimated by curve fitting.

The deterioration profiles obtained by this approach have the advantage that they are easy to use in analysis and design of reinforced concrete structures; see e.g. Ellingwood [1]. The disadvantage is that it is not easy to estimate the deterioration profiles for new structures and new materials, since the deterioration curves are not directly related to physical, mechanical, or chemical parameters.

In a more modern approach, the estimation of the deterioration is based on a detailed understanding of the chemical and physical processes that take place during deterioration. This approach is used in this paper but only deterioration related to corrosion of the reinforcement is considered. Other types of deterioration may be handled in a similar way. Corrosion of the reinforcement is one of the major reasons for deterioration of reinforced concrete structures.

Initially, the main effect of corrosion is a reduced strength of the structural element in question due to a reduced cross-section of the reinforcement. Another effect of the corrosion is the close interaction between corrosion and the bond between the concrete and the reinforcement. A reduced bond will also influence the structural strength of the structure and must therefore be included in a complete estimation of the

[1] Course-Workshop on "Optimal Bridge Maintenance Based on Risk and Reliability", Toluca, Mexico, August 11-13, 2008.

deterioration process. Important research on bonding is taking place in several research institutions; see e.g. Lundgren [2] and Maurel, Dekoster & Buyle-Bodin [3].

It is a serious problem that the volume of the rust products is higher than the volume of the corroded steel. The porous zone around the steel/concrete surface can to some extent absorb the higher volume of the rust products. However, at a certain time the total amount of corrosion products exceeds the amount of corrosion products needed to fill the porous zone around the reinforcement. The rust products will then create expansive pressure on the surrounding concrete. The expansion of the concrete near the reinforcement will initiate tensile stresses in the concrete. After some time with increasing corrosion the tensile stresses will reach a critical value and corrosion cracks may develop. With further production of rust, the crack opening will increase and eventually result in spalling. This last part of the corrosion process is still not well understood. More research is certainly needed to clarify these important problems for a corroded reinforced concrete structure.

This paper is primarily based on the papers Thoft-Christensen [25] and Thoft-Christensen, Frandsen & Svensson [26].

2. THE CHLORIDE INGRESS

Chloride-induced corrosion has been investigated by e.g. Neville [4]. Reinforced concrete is an excellent type of material from a corrosion point of view, since the alkaline environment in the concrete maintains a passive film on the surface of the reinforcement, and this film protects the reinforcement against corrosion. However, if the concrete is penetrated by e.g. water or carbon dioxide, then this passive film breaks down and the reinforcement is open to corrosion. An anodic region is established, where the passive film is broken down, whereby an electrochemical cell is formed. The passive surface is the cathode, and the electrolyte is the pore water in the concrete. At the anode the following reactions take place:

$$\begin{aligned} &Fe \rightarrow Fe^{++} + 2e^{-} \\ &Fe^{++} + 2(OH)^{-} \rightarrow Fe(OH)_2 \\ &4Fe(OH)_2 + 2H_2O + O_2 \rightarrow 4\,Fe(OH)_3 \end{aligned} \qquad (1)$$

Chloride ions Cl^{-} activate the unprotected surface and form an anode. The chemical reactions are

$$\begin{aligned} &Fe^{++} + 2Cl^{-} \rightarrow FeCl_2 \\ &FeCl_2 + 2H_2O \rightarrow Fe(OH)_2 + 2HCL \end{aligned} \qquad (2)$$

It follows from Eqs. (1) and (2) that two rust products $Fe(OH)_2$ and $Fe(OH)_3$ are produced in this case.

Corrosion product	*Color*	*Volume, cm^3*
Fe_3O_4	Black	2.1
$Fe(OH)_2$	White	3.8
$Fe(OH)_3$	Brown	4.2
$Fe(OH)_3,3H_2$	Yellow	6.4

Table 1. Volume of corrosion products corresponding to corrosion of 1 cm^3 Fe.

The different types of rust products are interesting to study because they have great influence on corrosion cracking, since the volume of the rust products

corresponding to a given volume of the steel varies a lot. This problem has been studied for several corrosion products by Nielsen [5]. He has obtained the rust volumes corresponding to corrosion of 1 cm^3 Fe, see Table 1.

3. THE CHLORIDE DIFFUSION PROCESS

The penetration of chloride ions into the concrete is difficult to model. Some simplifying assumptions are needed. There seems to be a general agreement that a model based on diffusion theory is a reasonably good approximation. If the chloride concentration C_0 on the surface of the concrete and the diffusion coefficient D for concrete are independent of space (location) and time, then Fick's law of diffusion can represent the rate of chloride penetration into concrete, as a function of depth from the concrete surface and as a function of time

$$\frac{\partial C(x,t)}{\partial t} = D\frac{\partial^2 C(x,t)}{\partial x^2} \tag{3}$$

where $C(x,t)$ is the chloride ion concentration, as % by weight of cement, at a distance of x cm from the concrete surface after t seconds of exposure to the chloride source. D is the chloride diffusion coefficient expressed in cm^2/sec. The solution of the differential equation (3) is

$$C(x,t) = C_0\left\{1 - \text{erf}\left(\frac{x}{2\sqrt{D\,t}}\right)\right\} \tag{4}$$

where C_0 is the equilibrium chloride concentration on the concrete surface, as % by weight of cement, erf is the error function.

The chloride ingress with a time-dependent chloride concentration at the concrete surface has been investigated by Frederiksen, Mejlbro & Poulsen [6] and by Mejlbro [7] on the basis of a solution of the diffusion law with time-dependent diffusion coefficient and time-dependent surface concentration. Mejlbro & Poulsen [8] have considered the special case where the time dependent chloride concentration on the surface is approximated by a piecewise set of linear functions versus time. Such an approach is relevant for e.g. bridges where de-icing salt containing chloride is used during the winter period.

It is further assumed that a corrosion process is initiated when the chloride concentration at the site of the reinforcement reaches a certain critical chloride corrosion threshold value C_{cr}. The critical chloride threshold depends on the type of concrete and several factors; see e.g. Frederiksen [9]. If C_{cr} is assumed to be the chloride corrosion threshold and d is the thickness of the concrete cover, then the corrosion initiation period T_{corr} can be calculated. The time T_{corr} to initiation of reinforcement corrosion is

$$T_I = \frac{(d_1 - D_1/2)^2}{4D_C}(erf^{-1}(\frac{C_{cr} - C_0}{C_i - C_0}))^{-2} \tag{5}$$

On the basis of equation (5) outcomes of the corrosion initiation time T_{corr} have been performed by simple Monte Carlo simulation on the basis of the data in table 2; see Thoft-Christensen [10].

A Weibull distribution can be used to approximate the distribution of the simulated data. The Weibull distribution is $W(x; \mu, k, \varepsilon)$, where μ = 63.67, k = 1.81

and ε = 4.79 . The corresponding histogram and the density function are shown in figure 1.

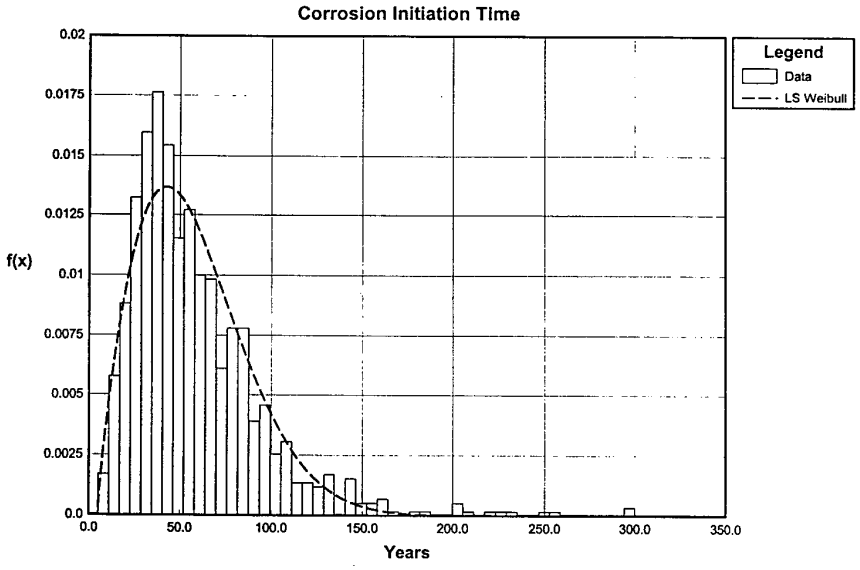

Figure 1. Density function of the corrosion initiation time T_{corr} , Thoft-Christensen [10].

Initial chloride concentration	0 %,
Surface chloride concentration	Normal (0.650 ; 0.038)
Diffusion coefficient	Normal (30 ; 5)
Critical chloride concentration	Normal (0.3 ; 0.05)
Cover	Normal (40 ; 8)

Table 2. Parameters used in the simulation study of T_{corr} .

4. THE DIFFUSION COEFFICIENT *D*

It follows from Eq. 5 that the time to corrosion imitation T_{corr} is inversely proportional to the diffusion coefficient *D*. It is therefore of great interest to get a good estimate of *D*. The diffusion coefficient *D* is not a real physical constant for a given concrete structure, since it depends on a number of physical factors. The most important factors are the water/cement ratio *w/c*, the temperature Φ, and the amount of e.g. silica fumes (s.f.); see Jensen [11] and Jensen, Hansen, Coats & Glasser [12].

The data presented in this section are all based on Jensen [11] and Jensen, Hansen, Coats & Glasser [12]. Figure 2 shows the diffusion coefficient *D* as a function of the water-cement ratio w/c and the temperature Φ °C for cement pastes with 0% silica fume. It is clear from figure 2 that the diffusion coefficient *D* increases significantly with *w/c* as well as the temperature Φ. In this example the minimum value of *D* is 0.31×10^{-12} m^2/s corresponding to *w/c* = 0.2 and the temperature Φ = 4°C. The maximum value of *D* is 80.00×10^{-12} m^2/s corresponding to *w/c* = 0.70 and Φ = 35 °C. In figure 3 the contour lines for the same data are shown.

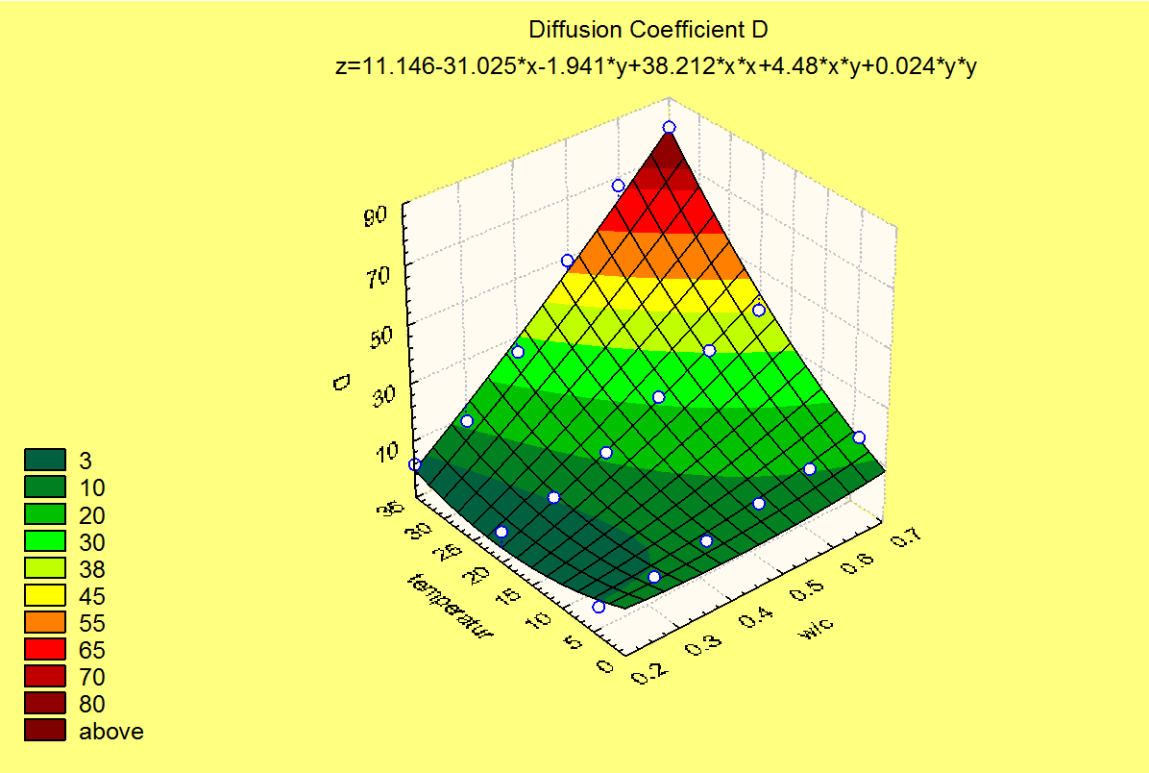

Figure 2. The diffusion coefficient D (10^{-12} m^2/s) as a function of *w/c* and of the temperature Φ, Thoft-Christensen [13].

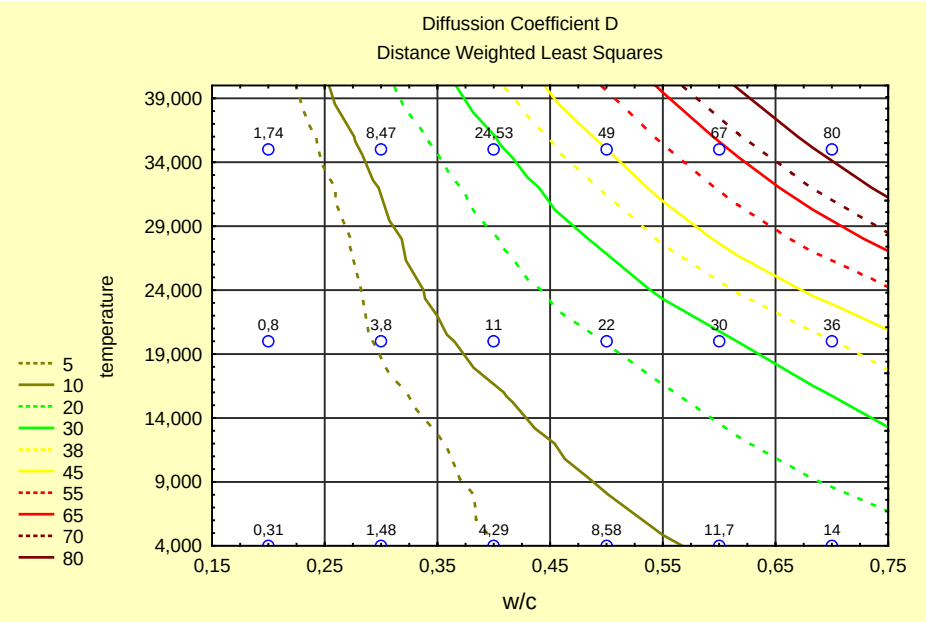

Figure 3. The diffusion coefficient D (10^{-12} m^2/s) as a function of the water-cement ratio w/c and the temperature Φ °C, Thoft-Christensen [13].

The addition of silica fume (s.f.) is of great importance for the chloride ingress. Silica fume additions reduce the chloride ingress because of changes in the pore

structure; see table 3 and Jensen [11].

w/c	0.3					0.5				
% s.f.	0	3	6	10	20	0	3	6	10	20
D (10^{-12}m/s)	3.8	2.0	0.42	0.12	0.05	22	13	4.2	1.6	

Table 3. The diffusion coefficient *D* as a function of % s.f. for two values of *w/c* and Φ =20 °C.

5. SITE DEPENDENCY OF THE DIFFUSION COEFFICIENT *D*

The data in section 4 clearly indicate that site information is needed to make e.g. an estimation of the remaining life cycle of a bridge or any estimation where the diffusion coefficient *D* is involved.

This has been confirmed by several authors see e.g. Suda et al. [14], where important information of the distribution of the diffusion coefficient *D* in Japan is shown. Figure 4 shows the mean air temperature Φ and the *w/c* ratio in Japan. As expected, the temperature is much higher (21-25°C) in the southern part of Japan than in the northern part (4-9°C). The w/c ratio has a smaller variation, but the highest ratios are in the Kanto area where also the temperature Φ is relatively high.

Figure 5 shows measured values of the diffusion coefficient *D* in Japan. The diffusion coefficient *D* nicely confirms the theoretical results in section 4, namely that D increases with *w/c* and with the temperature Φ.

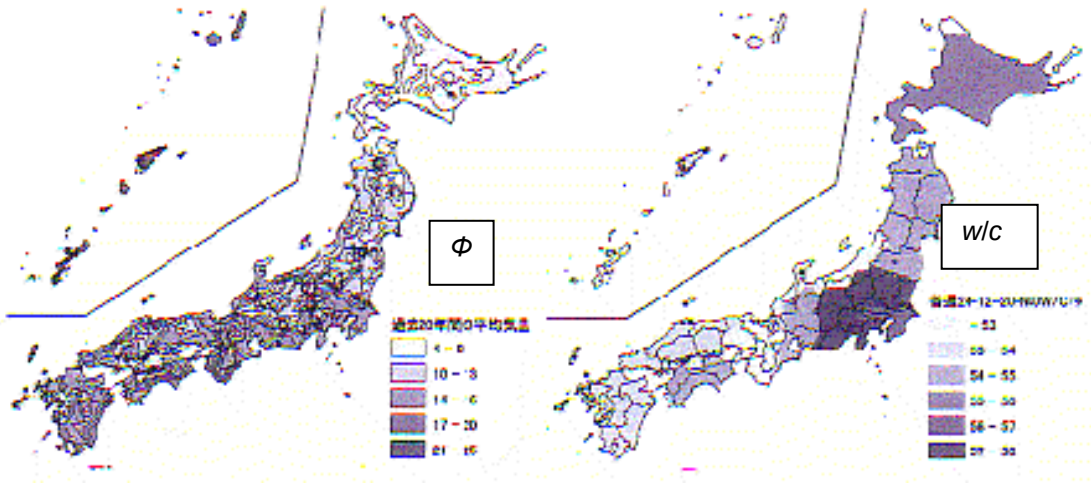

Figure 4. Mean air temperature Φ and *w/c* ratio in Japan (figures 3 and 5 in Suda et al. [14]).

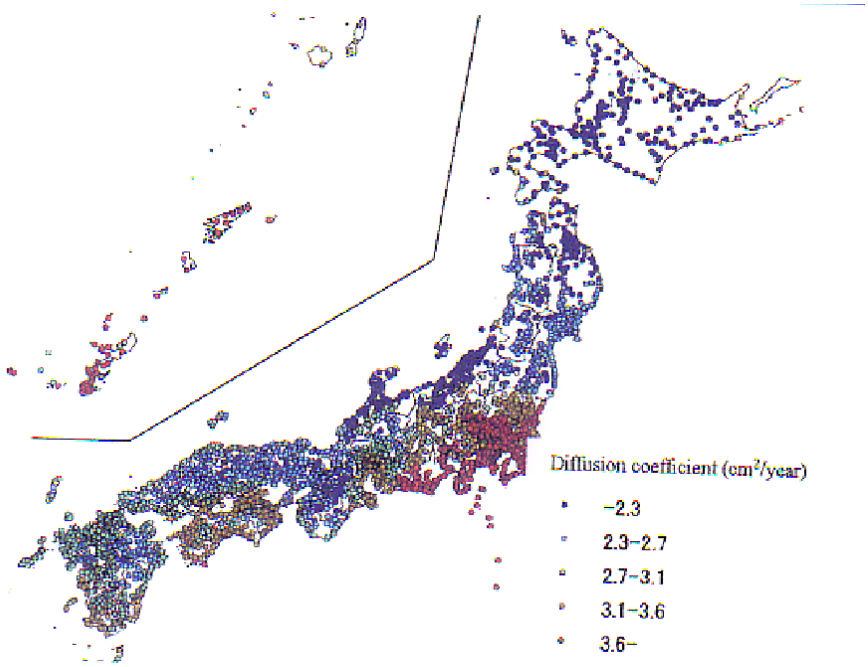

Figure 5. Distribution of the diffusion coefficient D (cm2/year) in Japan (Figure 15 in Suda et al. [14]).

6. BINDING MODIFIED DIFFUSION LAW

Fick's law for diffusion was used as early as 1970 for calculation of the diffusion coefficients for various concrete compositions; see Collepardi et al. [15]. Since then, Fick's law has been the basis for chloride ingress modeling, but a large number of modifications have been introduced, see Jensen [11]. Fick's diffusion law has e.g. been modified taking into account binding of chloride by assuming that the free chloride follows Fick's law; see Jensen [11] and Jensen et al. [12]. It is also assumed that the chloride binding follows a Freundlich isothermal equation; Luping [16].

$$c_b = \alpha \times c_f^{\beta} \tag{6}$$

where c_b [mg/n-gel] is the bound chloride, c_f [mol Cl/l solution] and α and β are empirical constants. The chloride binding significantly modifies the shape of the chloride ingress profiles as well as the calculated chloride diffusion coefficient *D*. In figure 6 the principal difference between chloride ingress profiles with and without binding is shown. Without bonding the profile is strongly concave and with binding the profile is almost linear. Generally, measured profiles are almost linear so a modeling with binding seems to be a great improvement.

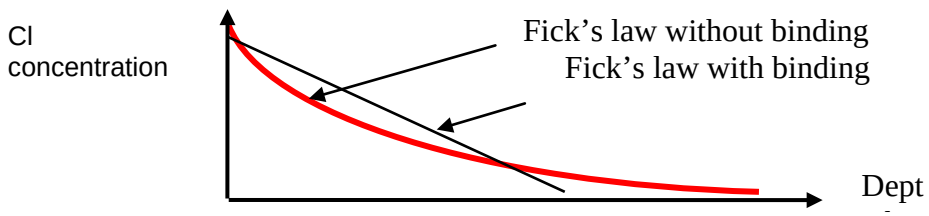

Figure 6. Chloride ingress profiles.

In Jensen [11] is presented an example that strongly supports this conclusion. A

cement paste with *w/c* = 0.3 and with no additives was exposed to chlorides for 30 days at 35°. Without binding the diffusion coefficient is $1.5 \times 10^{-12} m^2/s$ and with binding included the diffusion coefficient for the free chloride is $3.7 \times 10^{-12} m^2/s$. If binding is included the description is substantially improved.

7. THE *w/C* RATIO

The *w/c* ratio for an existing concrete element may be estimated using Optical Fluorescence Microscopy; see Jakobsen [17] and Concrete-experts [18]. Thin sections of the concrete are fluorescent impregnated and analyzed under an optical microscope using a combination of a blue excitation filter and a yellow blocking filter In fluorescent light the epoxy filled air voids and cracks then appear yellow. Cement paste appears as

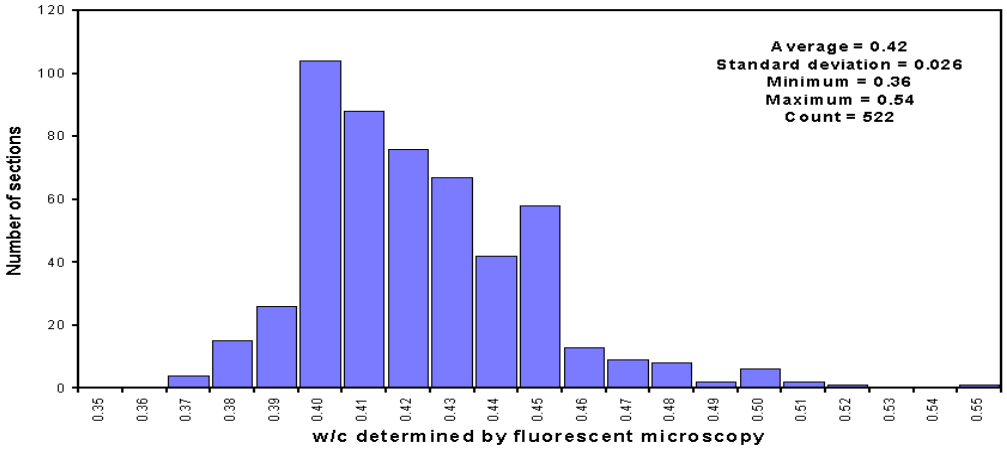

Figure 7. Distribution of w/c measure in 522 thin sections by fluorescence microscopy (Concrete-experts).

shades of green and aggregates black. The shade of green of the cement paste depends on the capillary porosity. A sample with a low w/c ratio appears dark green and a sample with high w/c ratio appears light green. These shades of green are use to estimate the w/c ratio by comparing with the colors of a standard cement pastes where the w/c ratios are known.

In figure 7 is shown the determination of the w/c ratio of precast railroad ties performed on 522 thin sections representing 127 ties. The average value is 0.42 and the standard deviation is 0.026 (the coefficient of variation is 6%).

8. THE TEMPERATURE *Φ*

The temperature *Φ* is modelled as a stochastic variable based on the temperature at the site of the structure. The modeling should take into account that the yearly mean temperature varies significantly from year to year. The data needed for the stochastic modeling are in most cases available from national meteorological institutions. In figure 8 is as example shown the yearly mean temperature in Denmark for the years 1873-2001, see Cappelen [19]. Notice that the mean yearly temperature in this time period varies between below 6°C to over 9°C and that there has been a significant increase in the mean yearly temperature. These facts can be taken into consideration by

weighting the estimated diffusion coefficient.

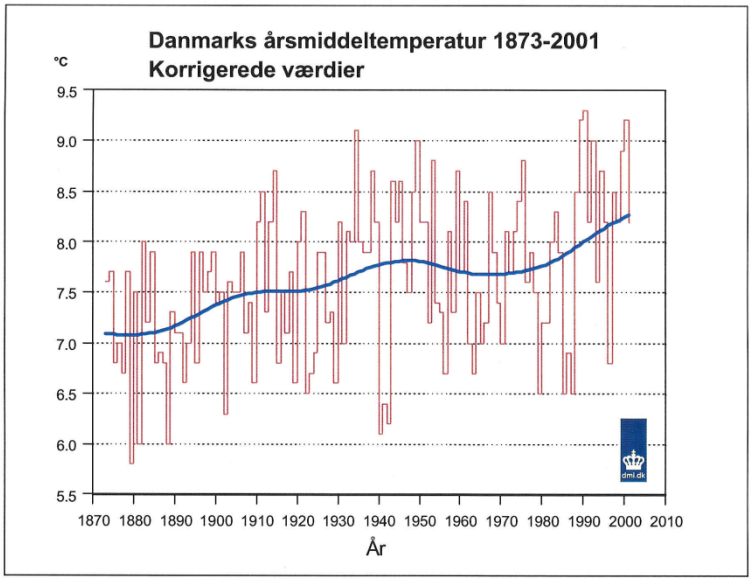

Figure 8. Yearly mean temperature for Denmark 1873-2001.

9. STOCHASTIC MODELLING OF THE DIFFUSION COEFFICIENT *D*

Based on the experimental results presented in section 4, the following formula may be used to approximately describe the diffusion coefficient D as a function of the w/c ratio and the temperature Φ:

$$D = 11.146 - 31.025\times W/C - 1.941\times\Phi + 38.212\times(W/C)^2 + 4.48\times W/C\times\Phi + 0.024\times\Phi^2 \quad (7)$$

As an example assume that w/c is log-normally distributed LN(0.45,0.02) and that the temperature Φ is normally distributed N(10.0°C , 1.0°C). Then by crude Monte Carlo simulation (10.000 samples) it may be shown that the diffusion coefficient may be modeled by a normally distributed stochastic variable N(8.11×10^{-12} m^2/s, 1.11×10^{-12} m^2/s), that is with a coefficient of variation equal to 14%.

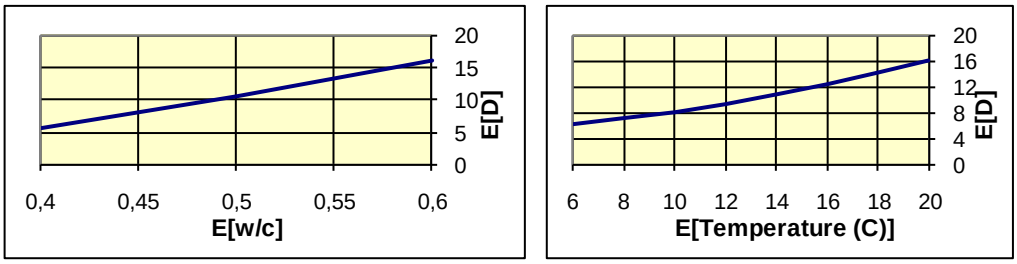

Figure 9. Sensitivity analysis with regard to the mean values of *w/c* and of the temperature Φ.

The diffusion coefficient D is, as expected, strongly sensitive to the mean values of *w/c* and Φ as shown in figure 9. In the diagram to the left, *w/c* is log-normally distributed LN(E[w/c],0.02) and the temperature Φ is normally distributed N(10.0°C , 1.0°C) and E[D] is the expected value of D. In the diagram to the right, *w/c* is log-normally distributed LN(0.45,0.02) and the temperature Φ is normally distributed

N(E[Temperature] , 1.0°C).

The standard deviation std[*D*] of the diffusion coefficient *D* (but not the expected value E[*D*]) is sensitive to the standard deviations of w/c and Φ as shown in figure 10. In the diagram to the left, w/c is log-normally distributed LN(0.45,std[w/c]) and the temperature Φ is normally distributed N(10.0°C , 1.0°C). In the diagram to the right, w/c is log-normally distributed LN(0.45,0.02) and the temperature Φ is normally distributed N(10^0C , std[temperature]).

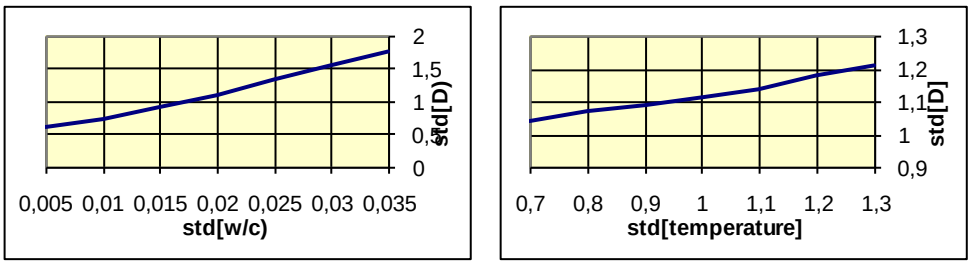

Figure 10. Sensitivity analysis with regard to the standard deviations of *w*/*c* and of the temperature.

10. INITIATION OF CORROSION CRACKS

The corrosion process after corrosion initiation is very difficult to model, since a large number of changes in the rebars as functions of the time have been observed and reported in the literature. The simplest model is to assume that the diameter $d(t)$ of the reinforcement bars at the time $t>T_{corr}$ is modelled by

$$d(t) = d_0 - c_{corr} i_{corr} (t - T_{corr}) \tag{8}$$

where d_0 is the initial diameter, c_{corr} is a corrosion coefficient, and i_{corr} is the rate of corrosion. Based on a survey, three models for chloride penetration have been proposed (the initial chloride concentration in the concrete is assumed to be zero): low, medium, and high deterioration; see Thoft-Christensen & Jensen [20].

There is a porous zone around the steel/concrete surface caused by the transition from paste to steel, entrapped/entrained air voids, and corrosion products diffusing into the capillary voids in the cement paste. When the total amount of corrosion products exceeds the amount of corrosion products needed to fill the porous zone around the steel, the corrosion products create expansive pressure on the surrounding concrete. Close to reinforcement bars the concrete has some porosity. Very close to the bars the porosity is close to 1, but the porosity decreases with the distances from the bars. The porosity is typically of the order of 0.5 about 10 - 20 μm from the bars.

Let t_{por} be the thickness of an equivalent zone with porosity 1 around a steel bar, and let t_{por} be modelled by a lognormal distribution with the mean 12.5 μm and a standard deviation of 2.54 μm. Further, let the density ρ_{rust} of the rust product and the initial diameter d_0 be modelled by normal distributions N(3600,360) kg/m^3 and N(16,1.6) mm, respectively.

Then it can be shown by Monte Carlo simulation that the volume of the porous zone W_{porous} with a fairly good approximation can be modelled by a shifted lognormal distribution with a mean 2.14e−03 kg/m, a standard deviation 0.60e−03 kg/m and a

shift of 0.82e – 03 kg/m; see Thoft-Christensen [10].

After a certain time the rust products will fill the porous zone completely and then result in an expansion of the concrete near the reinforcement. As a result of this, tensile stresses are initiated in the concrete. With increasing corrosion the tensile stresses will reach a critical value and cracks will be developed. During this process the corrosion products at initial cracking of the concrete will occupy three volumes, namely the porous zone W_{porous}, the expansion of the concrete due to rust pressure W_{expan}, and the space of the corroded steel W_{steel}. The corresponding total amount of critical rust products W_{crit} needed to fill these volumes is

$$W_{crit} = W_{porous} + W_{expan} + W_{steel} \tag{9}$$

Using Monte Carlo simulation it can be shown that W_{expan} with a good approximation can be modelled by a normal distribution N(0.0047 , 0.0011) kg/m when the data shown above are used; see Thoft-Christensen [10]. Finally, W_{steel} can be written

$$W_{\text{steel}} = \frac{\rho_{\text{rust}}}{\rho_{\text{steel}}} M_{\text{steel}} \tag{10}$$

where ρ_{steel} is the density of steel and M_{steel} is the mass of the corroded steel. Clearly, M_{steel} is proportional to W_{crit}.

Liu & Weyers [21] have calculated the factor of proportionality for two kinds of corrosion products as 0.523 and 0.622. For simplicity, it will be assumed that $M_{steel} = 0.57 W_{crit}$. Therefore, Eq. 8 can be rewritten

$$W_{crit} = \frac{\rho_{steel}}{\rho_{steel} - 0.57\rho_{rust}} (W_{porous} + W_{expan}) \tag{11}$$

Let ρ_{steel} be modelled by a normal distribution N(8000 ; 800) kg/m^3. Then by Monte Carlo simulation it can be shown that W_{crit} with a good approximation can be modelled by a normal distribution N(0.010 ; 0.0027) kg/m; see Thoft-Christensen [10]. The rate of rust production as a function of time *t* (years) from corrosion initiation can be written, Liu & Weyers [21]

$$\frac{dW_{rust}(t)}{dt} = k_{rust}(t) \frac{1}{W_{rust}(t)} \tag{12}$$

i.e. the rate of corrosion is inversely proportional to the amount of rust products W_{rust} (kg/m). The factor $k_{rust}(t)$ (kg^2/m^{2}year) is assumed to be proportional to the annual mean corrosion rate $i_{cor}(t)$ (μA/cm^2) and the diameter *d* (m) of the reinforcement. The proportionality factor depends on the types of rust products, but is here taken as 0.383e – 3.

$$k_{rust}(t) = 0{,}383 \times 10^{-3} d i_{corr}(t) \tag{13}$$

By integration

$$W_{rust}^2(t) = 2 \int_0^t k_{rust}(t) dt \tag{14}$$

Let $i_{cor}(t)$ be modelled by a time-independent normally distributed stochastic variable N(3 ; 0.3) (μA/cm^2) then the time from corrosion initiation to cracking Δt_{crack}

can be estimated by (16) by setting $W_{rust}(\Delta t_{crack}) = W_{crit}$.

$$T_{crack} = \frac{W_{crit}^2}{2k_{rust}} = \frac{W_{crit}^2}{2 \times 0.383 \times 10^{-3} D\, i_{corr}} \tag{15}$$

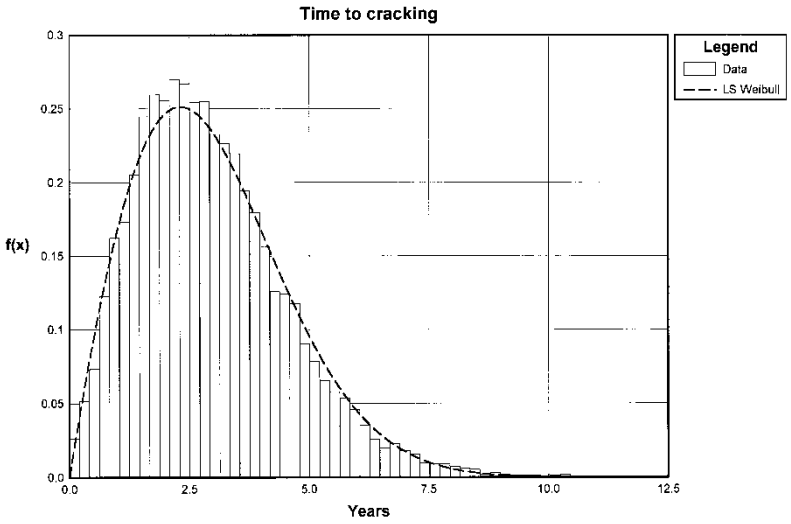

Figure 11. Density function of Δt_{crack}, Thoft-Christensen [10].

Then it can be shown by Monte Carlo simulation that Δt_{crack} with a good approximation can be modelled by a Weibull distribution W(3.350 ; 1.944 ; 0) years, see figure 11. The mean is 2.95 years and the standard deviation is 1.58 years. The mean value of T_{crack} is of the same order as the experimental values (and the deterministic values) obtained by Liu & Weyers [21].

11. THE CRACK - CORROSION INDEX

11.1 Introduction

Determining the reliability of reinforced concrete structures, based on visual inspection of corroding cracks on the surfaces of structures, is of great interest. In the present study, models for the deterioration of reinforced concrete structures are presented with special emphasis on a model for the corrosion crack opening. Experiments and theoretical analysis by a numerical final element method (FEM), support that the reduction of the reinforcement bar diameter due to corrosion is proportional to the corresponding increase in crack width, measured on the surface of a concrete specimen, for a given time interval.

More recently, the constant of proportionality, the so-called crack-corrosion index, has been studied further with respect to its dependence on the diameter of the reinforcement and the concrete cover. In this section, the above work is presented and extended with more realistic 3D-models of the cracked concrete beam. The crack-corrosion index is evaluated for variations of different parameters, such as bar diameter, concrete cover, crack length, and type of corrosion product.

11.2 Crack-corrosion experiments

Several researchers have investigated the evolution of corrosion cracks in reinforced concrete beams experimentally, e.g. Andrade et al. [22]. To reduce the duration of testing, artificial corrosion by electrical current is a common experimental approach. During the test, the loss of rebar cross-section is monitored and the corresponding crack evolution is measured by strain gauges attached to the surface of the specimen. In the study by Andrade et al. [22], four simple test specimens were investigated. The specimens were small reinforced concrete beams with only a single rebar with a 20 or 30 mm concrete cover. In figure 12, the results from this experimental study are shown.

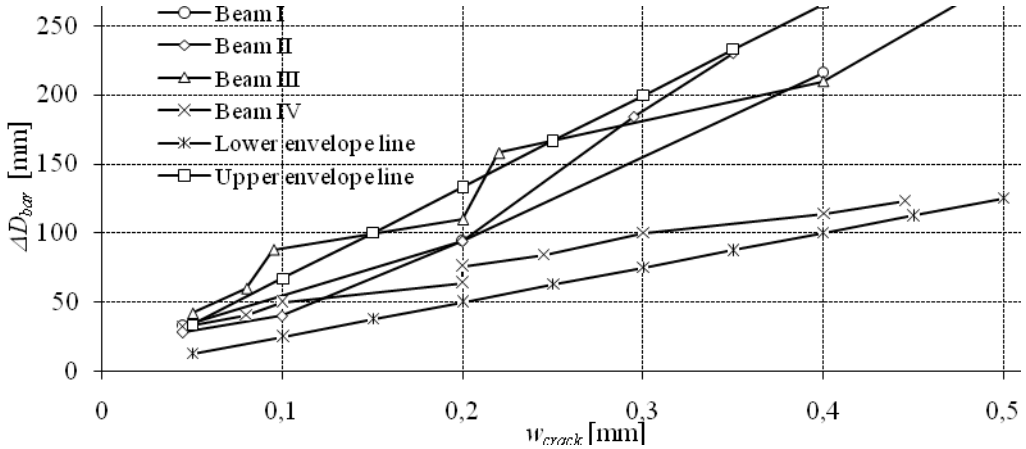

Figure 12. Reduction of rebar diameter ΔD_{bar} versus the crack width w_{crack}, based on data in Andrade et al. [22].

After formation of the initial crack, the rebar cross-section is further reduced due to the continued corrosion, and the width of the crack is increased as shown in figure 12. In all four experiments by Andrade et al. [22], proportionality between the reduction of the rebar diameter ΔD_{bar} and the maximum crack Δw_{crack} width measured at the surface of the concrete specimen is found:

$$\Delta w_{crack} = \gamma \Delta D_{bar} \tag{16}$$

where the crack-corrosion index γ is the constant of proportionality. From the experiments shown in figure 12, the upper and lower bound for γ is determined as being of the order 1.5 to 5.

11.3 Estimating the crack-corrosion index γ

A simple method for estimating the crack-corrosion index by considering the shape changes of a crack and by the color of observed corrosion product is now presented. Assuming small changes of geometry $\Delta D << D$ and that the corrosion products are constrained to the domain, an approximate relation between the decrease of the steel bar diameter ΔD_{bar} and the increase of the hole diameter ΔD_{hole} may be determined. This is carried out by an analysis of the change of geometry from the initial state shown in figure 13a, to a state where corrosion has continued and more rust products are present; see figure 13b. The volume of generated rust per length ΔA_{rust} of these products is determined from the decrease of the steel bar diameter as

$$\Delta A_{rust} = \alpha \frac{\pi}{2} \Delta D_{bar} D_{bar} \tag{17}$$

where α is the volume fraction between steel and rust product; see table 1.

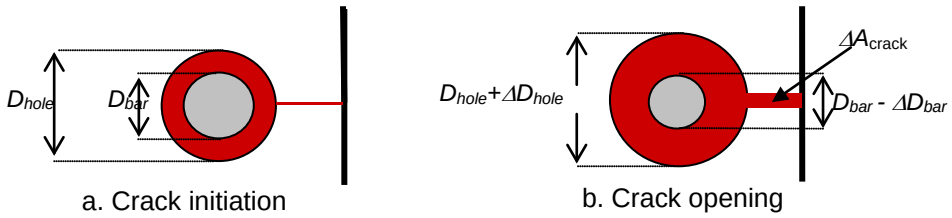

Figure 13. Schematic illustration of the notations displayed on the crack shown at two different stages of the cracking.

The total increase of the volume per length due to cracking, ΔA_{exp}, results from reduction of bar diameter ΔD_{bar}, expansion of the hole diameter ΔD_{hole}, and increased crack opening ΔA_{crack} and may be written as

$$\Delta A_{exp} = \frac{\pi}{2} \Delta D_{bar} D_{bar} + \frac{\pi}{2} \Delta D_{hole} D_{hole} + \Delta A_{crack} \tag{18}$$

With the additional assumption that at crack initiation $D_{bar} \approx D_{hole}$, the cross sectional areas found in equations (17) and (18) ΔA_{rust} ΔA_{exp} are identical, and the relation between reduction of steel bar diameter and expansion of hole diameter becomes

$$(\alpha - 1)\Delta D_{bar} \approx \Delta D_{hole} + \frac{2\Delta A_{crack}}{\pi D_{hole}} \tag{19}$$

and, from the definition of the crack corrosion index

$$\gamma = \frac{\Delta w_{crack}}{\Delta D_{bar}} \approx (\alpha - 1) \frac{\Delta w_{crack}}{\Delta D_{hole} + 2\Delta A_{crack} / \pi D_{hole}} \tag{20}$$

To estimate the shape changes of crack, a series of 2D and 3D FEM-simulations have been performed. The results of these are presented in the sections 11.4 and 11.5 respectively.

11.4 2D-modelling of the expanding crack in a beam cross-section

The first simulations of the crack-corrosion index γ by a FEM analysis, was presented at the IFIP TC7 Conference on "System Modelling and Optimization" in Sophia Antipolis, France, July 2003, using the commercial FEM program FemLab; see Thoft-Christensen [23]. A rectangular beam cross-section with only one reinforcement bar was considered, see figure 14. The diameter of the hole around the rebar at the time of crack initiation was D_{hole} = 20 mm and the cover was c = 10 mm. The initial crack width was 0.01 mm.

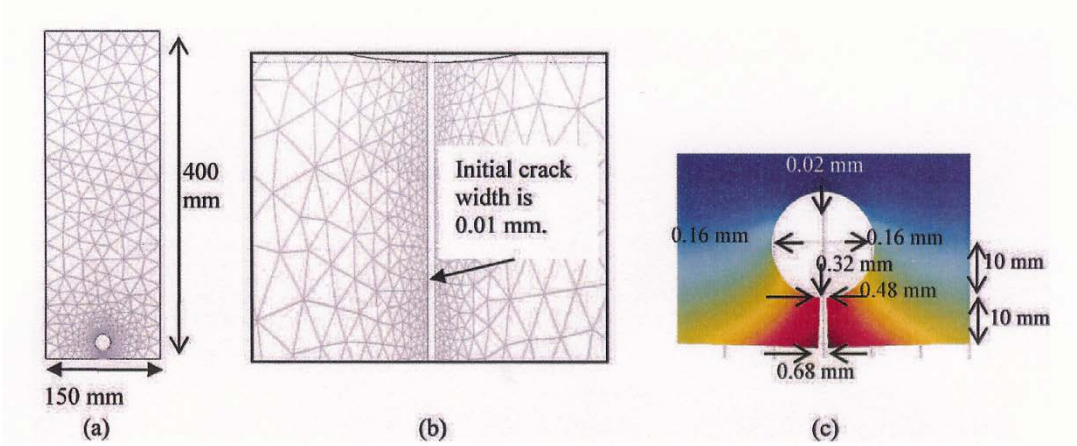

Figure 14. (a) the total FEM-mesh, (b) the local FEM-mesh in the vicinity of the crack, and (c) the calculated displacement field; Thoft-Christensen [23].

In the FEM model the rectangular cross-section in a long beam (plain strain) is assumed to have a centrally located reinforcement. A circular void, i.e. a hole, represents the reinforcement, and a initial crack with the width of 0.01 mm runs normal to the perimeter of the hole to the closest boundary of the concrete cross-section. The material is modelled as isotropic and linear elastic with a Young's modulus of $E = 25 \times 10^9$ Pa and Poisson's ratio of 0.2. Furthermore, the pressure caused by the expansion of corrosion products is represented by a uniform pressure normal to the perimeter of the hole. The magnitudes of pressure and Young's modulus are not important, since only the shape changes of the cross section in the elastic range are investigated.

Crack propagation can be modeled by an elasto-plastic constitutive law in combination with a suitable fracture criterion. These can be implemented in numerical methods such as X-FEM, or a meshless method. In stationary cracks, such as those studied here, no energy release from the cracking takes place. Furthermore, the high inelastic strains occur in a localized crack propagating zone at the crack ends and contribute very little to the deformations normal to the perimeter The deformations occurring in this stationary crack mat therefore be modeled by a linear elastic model to a good approximation.

For the example shown in figure 4, with a crack opening Δw_{crack} = 0.67 mm and an average increase of the hole diameter ΔD_{hole} = 0.31 mm the crack-corrosion index γ may be determined by equation (5) as

$$\gamma \approx (\alpha - 1)\frac{0.67}{0.31 + 2 \cdot 5.7/20\pi} = 1.36(\alpha - 1) \qquad (21)$$

or the crack-corrosion index is equal to 1.5 and 4.4 for black and brown rust, respectively; see table 3. This is in good agreement with the values obtained by the experiments by Andrade et al. [9] in section 2.

The results of a similar FEM analysis of a cross-section similar to the one illustrated in figure 14 were presented for 10 different combinations of the cover c and the diameter D_{bar} in Thoft-Christensen [26]. The conclusion from that study, where the cover was smaller than the rebar diameter, is that γ increases with the cover c for a fixed rebar diameter D_{bar}, and that γ also increased with the diameter D_{bar} for a fixed cover c.

Table 4. Estimates of $\gamma(D_{bar},c)$.

Diameter D_{bar}, mm	Cover c, mm				
	20	25	30	35	40
10	3.72	3.53	3.39	3.30	3.25
12	3.93	3.76	3.63	3.55	3.50
14	4.09	3.94	3.83	3.75	3.71
16	4.20	4.08	3.99	3.92	3.88
18	4.26	4.19	4.11	4.06	4.03
20	4.28	4.27	4.21	4.18	4.15

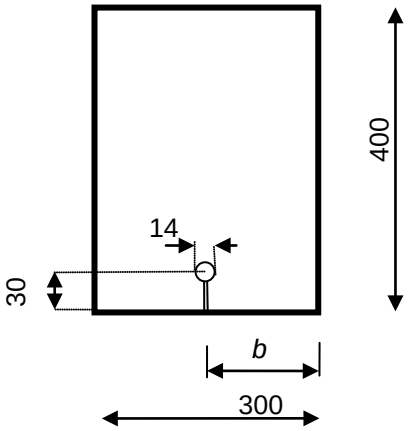

Figure 15. Cross-sectional dimensions with initial crack width of 0.01 mm (all dimensions in mm).

A similar analysis with 30 combinations of D_{bar} and c, where the cover was larger than the rebar diameter, but with a different cross-section confirms this conclusion; see Thoft-Christensen [13]. The crack-corrosion indices γ for the 30 combinations are shown in table 2 for black rust. It is seen that γ for the analysed combinations increases with the diameter D_{bar} and decreases with the concrete cover c.

In the same paper the significance of the distance b from the crack to the nearest uncracked vertical side of the beam was important for the estimate of crack-corrosion index γ. The same cross-section was used, but the hole and the crack were placed at different distances b from the vertical side of the beam, see figure 15.

As an example of the results from this investigation by Thoft-Christensen [23], a rebar, with diameter D_{bar} = 14 mm and concrete cover c = 30 mm, and a variation of $\gamma(b) \approx \eta(b)$, where $\eta(b) = \Delta w_{crack}/\Delta D_{hole}$ for the distances b = 30, 60, 90, 120, and 150 mm is shown in figure 16. In this figure, $\eta(b)$ is shown as a function of b.

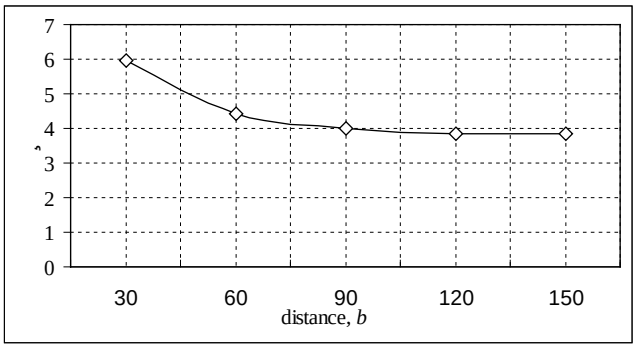

Figure 16. The function $\gamma(b) \approx \eta(b) = \Delta w_{crack}/\Delta D_{hole}$ for different distances, b , (mm) to the vertical edge.

The conclusion of this investigation is that the distance b to the vertical side of the beam is significant, if b is smaller than four times the rebar diameter. Otherwise, $\gamma(b) \approx \eta(b) = \Delta w_{crack}/\Delta, D_{hole}$ seems to be a good approximation.

11.5 3-D modeling of an expanding crack

In this section, the procedure used in the 2D model of corrosion crack evolution is extended to a 3D model. The 2D model in section 3 is based on several assumptions, e.g. that the movement of corrosion products is restricted to the cross-section considered. In a 3D mode, the corrosion products may also move in the direction of the reinforcement. Furthermore, in a 3D model it is possible to consider situations where only parts of the reinforcement are corroded.

A beam element with the dimensions $400 \times 800 \times 1000$ mm is considered for the illustration of the FEM model. The size of the beam is of minor importance, as long as the influence of the boundary conditions can be neglected, as in the chosen setup. The model contains one centered rebar with the diameter D_{bar} and with a concrete cover c, see figure 16. Corrosion is positioned in the central part of the reinforcement with the length l ($0 < l < 1000$ mm). An initial crack connects the corroded part of the reinforcement with the surface of the beam as shown in figure 17. Corrosion is positioned in the central part of the reinforcement with a length l ($0 < l < 1000$ mm). An initial crack connects the corroded part of the reinforcement to the surface of the beam.

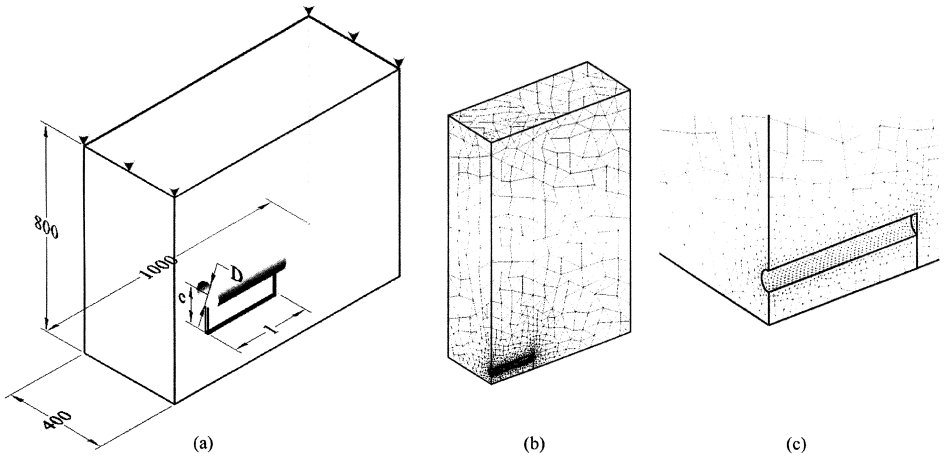

Figure 17. (a) The chosen boundary conditions for the FEM element model
(b) The FEM-mesh for one quarter of the considered beam
(c) The FEM-mesh near the corroded reinforcement and the crack.

In the FEM model, the beam has a cylindrical hole at the location of the corroded reinforcement and an initial crack (0 mm thick) from the hole to the boundary. The material outside the hole and the crack is modelled as isotropic and linear elastic with a Young's modulus of $E = 25 \times 10^9$ Pa and Poisson's ratio of 0.2. Furthermore, a uniform pressure applied normal to the cylindrical perimeter of the hole represents the pressure from the expansion caused by corrosion products. As a result of the symmetry, the FEM analysis is conducted on a quarter of the beam element considered.

11.6 Qualitative considerations of the shape changes of the crack

An important observation made under the numerical study of the crack opening was that, for different crack lengths, the influence of the remaining strength of the adjacent uncracked cross-sections was significant for the shape of the crack. The crack openings for four selected crack lengths are illustrated in figure 18.

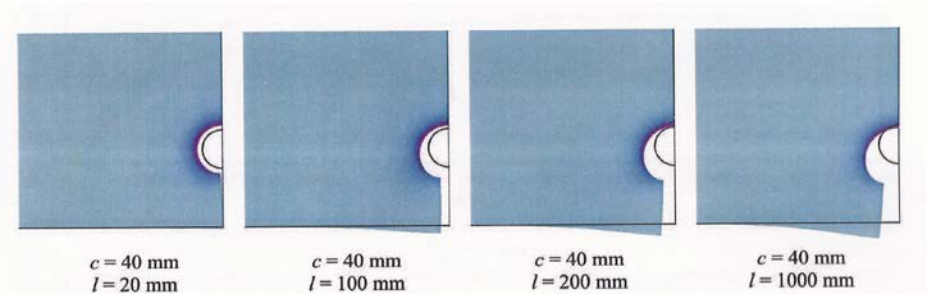

Figure 18. Illustration of the hole and the crack profile for 4 different lengths of the corroded part of the rebar. D_{bar}=20 mm.

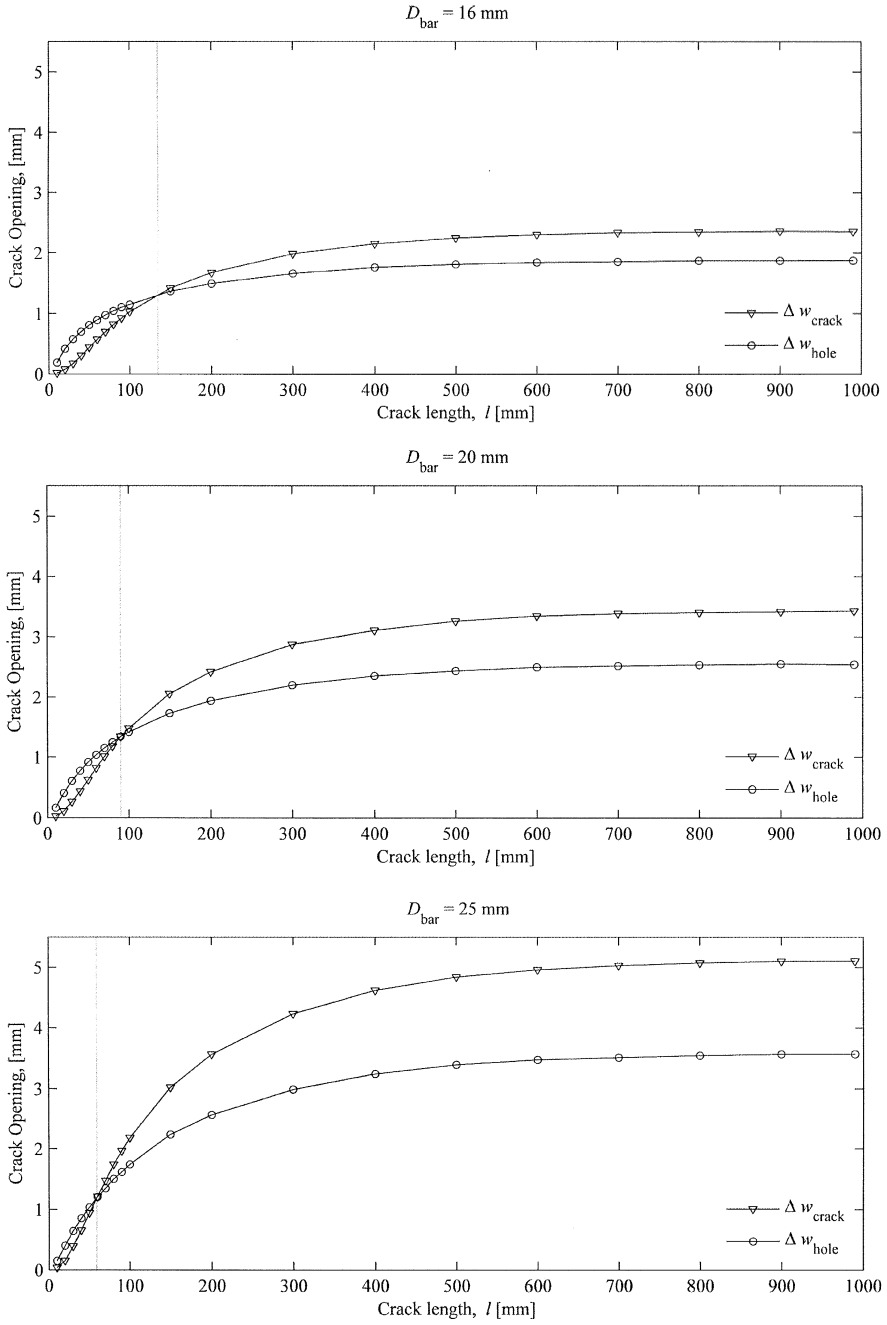

Figure 19. The crack openings for a beam with 40 mm cover at the surface Δw_{crack} and near the hole Δw_{hole} as a function of the crack length l.

The increases in crack openings at the surface Δw_{crack} and near the hole Δw_{hole} as a function of the crack length l are shown in figure 19. It can be noted that Δw_{crack} - Δw_{hole} is positive for l > 135, 90 and 60 mm for D_{bar} = 16, 20 and 25 mm, for a 40 mm cover respectively.

11.7 Numerical estimation of the crack-corrosion index

In this section, the crack corrosion index is estimated from the shape changes of 3D FEM models with different bar diameters, covers, and crack lengths. The FEM analysis is performed with 5 covers c = 20, 30,…, 60 mm for 20 different crack lengths l = 10, 20,…, 100, 200,…, 1000 mm and for 3 different rebar diameters D_{bar} = 16, 20 and 25 mm. This is an extension of the investigation in Thoft-Christensen et al. (2005), which includes the variations of cover and crack length but with one rebar diameter on 20 mm. In figure 20, two different series of calculations of the crack corrosion index are shown. To the left the crack corrosion index based on the shape changes of the middle section and to the right based on an average of the cross sections shape changes in the entire crack. In figure 20, the data are represented with a 3D-plot and contour curves for easy reading of γ- values.

Note that the crack-corrosion index γ decreases with increasing values of the cover. The curves in figure 20 are obtained by a regression analysis, which is presented in the next section.

11.8 Estimation of the crack-corrosion index γ by curve fitting

A simple least-square regression analysis has been performed on the crack-corrosion index γ estimation shown in figure 18. The chosen regression formulas are

$$\gamma = \left(F_1^{\beta} \exp\left(F_2^{\beta} (1-l)^{F_3^{\beta}} \right) + F_4^{\beta} \right)(\alpha - 1) \tag{22}$$

$$F_i^{\beta} = f_{i1}^{\beta} + f_{i2}^{\beta} D + f_{i3}^{\beta} c + f_{i4}^{\beta} D^2 + f_{i5}^{\beta} D c + f_{i6}^{\beta} c^2 \quad \text{for} \quad i \in \{1,2,3\} \quad \beta \in \{m,e\} \tag{23}$$

where β may be either m or e corresponding to the coefficient for γ calculated for the middle section or γ calculated as a average for all the sections in the entire crack. The components of f_{ij}^{β} is given in following matrices

$$\mathbf{f}^m = \begin{bmatrix} 2.22 & 1.43e2 & -8.79e1 & -2.13e3 & 2.03e2 & 5.57e2 \\ -2.25e-1 & -1.83e1 & -2.16e1 & 9.06e2 & -2.90e2 & 2.13e2 \\ 4.39e1 & 6.30e2 & -1.30e3 & -5.72e3 & -5.59e3 & 1.17e4 \\ 1.64e-1 & 2.80e1 & -6.32 & 2.23e2 & -1.59e2 & 9.87e1 \end{bmatrix} \tag{24}$$

$$\mathbf{f}^e = \begin{bmatrix} 2.25 & 1.24e2 & -8.89e1 & -1.46e3 & -1.00e2 & 6.44e2 \\ 1.76e-1 & -6.20e1 & -1.90e1 & 1.93e3 & -2.64e2 & 1.63e2 \\ 3.18e1 & 6.91e2 & -8.97e2 & -1.34e4 & -1.23e3 & 7.28e3 \\ 1.02e-2 & 9.07e1 & -1.10e1 & -1.88e3 & 5.03e2 & -3.37e1 \end{bmatrix} \tag{25}$$

The curves corresponding to (22) to (25) for α = 4.2 are shown in figure 21.

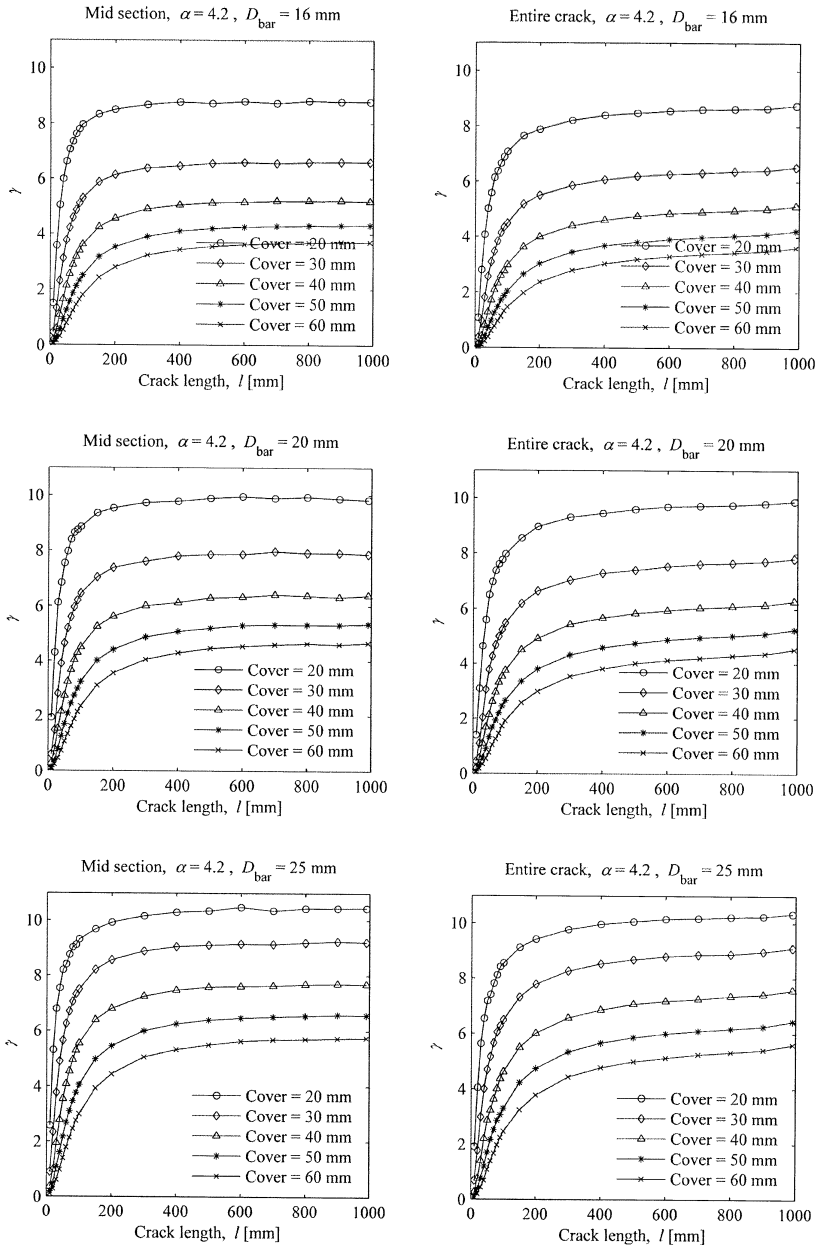

Figure 20. The crack-corrosion index γ as a function of the length of the corroded part of the rebar l, cover c and rebar diameter D_{bar} for the center cross section to the left and an average for the entire crack to the right. The symbols ○, ◊, Δ, * and × correspond to covers on 20, 30, 40, 50, and 60 mm, respectively. The curves are based on the regression analysis shown in section 11.8.

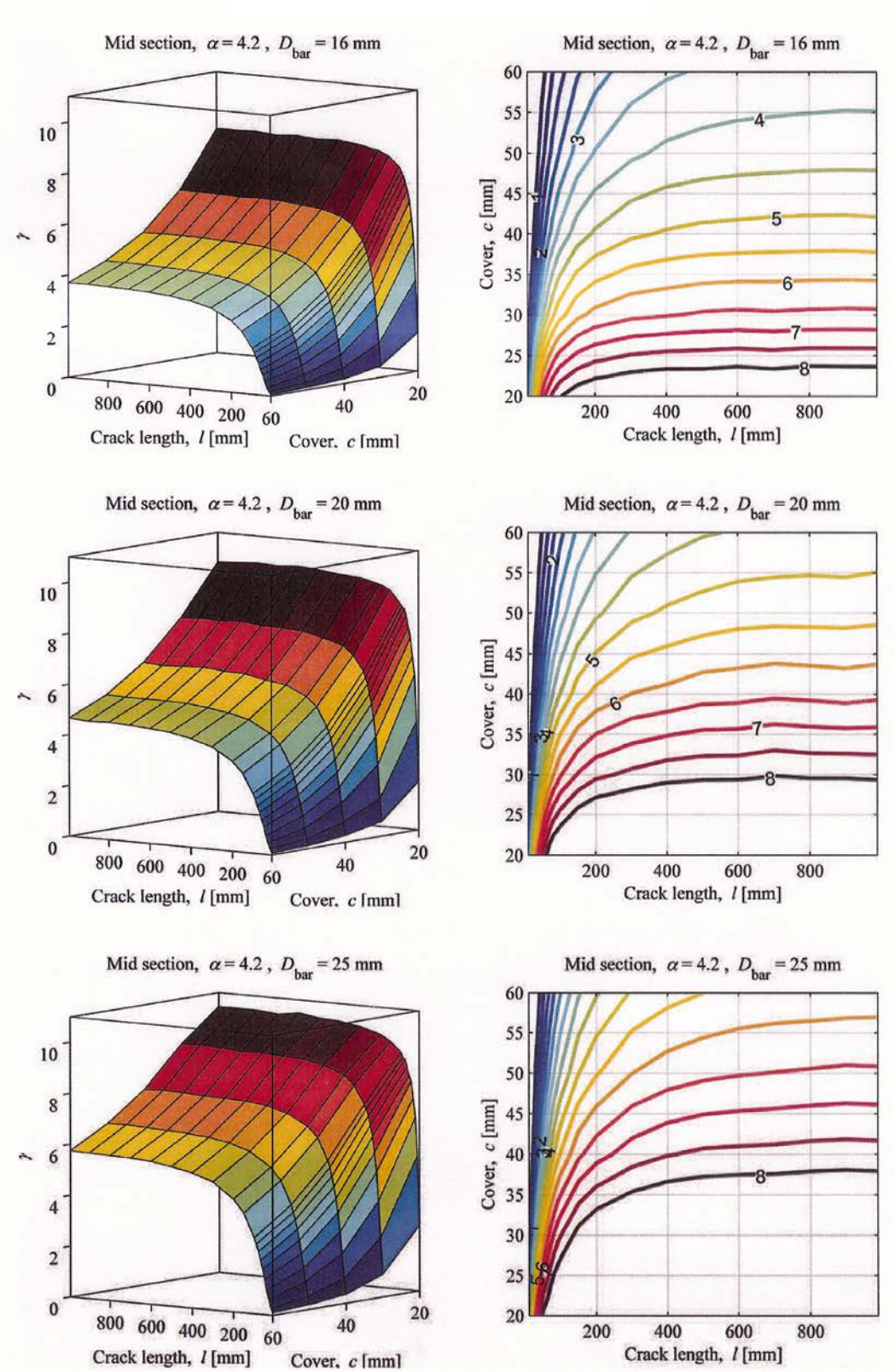

Figure 21. The crack-corrosion index γ as a function of the length of the corroded part of the rebar l, cover c and rebar diameter D_{bar} for the center cross section.

11.9 Pit Corrosion

In figure 21, the displacements are shown for the relatively short crack length l = 20 mm (pit corrosion), D_{bar} = 20 mm, and the cover is 40 mm. Note that the increase of the crack volume per length ΔA_{crack} (see figure 22) is small compared with cylindrical volume around the corroded part of the rebar.

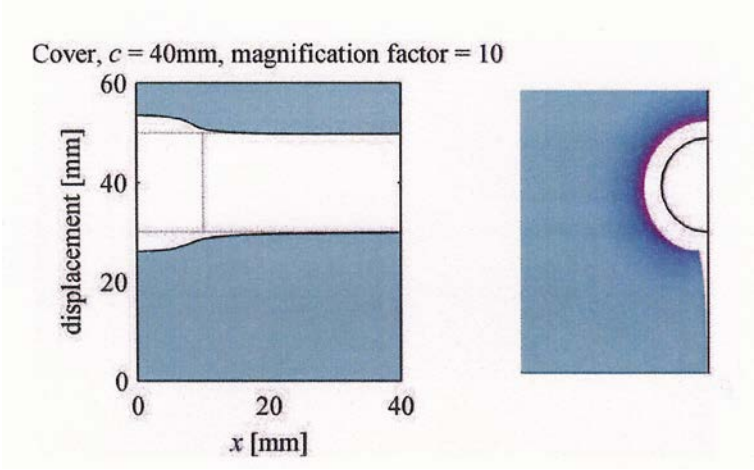

Figure 22. The displacement fields parallel and normal to the rebar for a short crack (pit corrosion).

The crack-corrosion index estimates shown in figure 21 indicate that the index γ varies moderately when the corrosion length l is greater than 300 mm of the length of the beam. However, for small values of l the index γ is reduced drastically. For very small values of l the index γ approaches zero. It can therefore be concluded that the approach used in this paper is not useful in the case of pit corrosion. This is as expected since the stiffness of the beam near the pit corrosion is very high as the pit corrosion crack is of little influence on the stiffness.

11.10 Conclusions on the crack corrosion index

Models for the deterioration of reinforced concrete structures are presented with special emphasis on the corrosion crack opening during corrosion of the reinforcement. Experiments and 2-dimensional FEM analysis support that the relation between the reduction of the reinforcement diameter ΔD_{bar} and the corresponding increase in crack width Δw_{crack}, measured on the surface of the concrete specimen may be approximated by a linear function. In this paper, the crack-corrosion index has been extended to more realistic 3D-models of the cracked concrete beam. The crack corrosion index may then be evaluated for a 3-dimensional beam by assuming a concentrated corrosion area of the reinforcement.

It has been shown that by equalizing the volume of the produced rust products with the volume due to the expansion of the hole and the increased crack volume, the reductions of the rebar cross-sectional area and thereby the safety of the beam may be estimated. The results presented in this paper are preliminary outputs of an ongoing research.

For multiple cracks located along adjacent rebars, the method may be applied if the debars are more than three times the diameter, since the stress field contributing to the deformations at this distance is negligible. For closer located rebars further investigations and research must be performed.

12. CONCLUSIONS

During the last 20-30 years, the interest in improving the modelling of deterioration of structural materials has been growing in all countries. Hundreds of papers have been published in material science journals and in all kind of engineering journals. A great number of conferences and meetings have been organized. New materials with interesting properties have been developed and new types of exciting structures have been designed. Very tall buildings, offshore structures, long bridges etc. are new challenges for architects and engineers. All this combined with a need to maintain the infrastructures everywhere have shown a need for a more precise and reliable description of strength and deterioration of structural materials.

In this paper the deterioration of reinforced concrete structures is presented with special emphasis on chloride penetration of the concrete. The first sign that something is wrong with a reinforced structure is often corrosion cracks leading to spalling and eventually to failure of the structure. However, corrosion-based failure is only one of several failure modes, but in many countries it is one of the most important types of failure.

It is therefore of great interest to design a reinforced concrete structure so that corrosion is not likely to take place in the planned lifetime of the structure, say 100 years. Especially structures near or in the sea and bridges, where de-icing is used, have a high risk of failure. It is therefore of great importance to understand the chemical, physical, and mechanical properties of reinforced materials. To this purpose a great number of deterministic and stochastic models for deterioration of reinforced structures have been developed. Some models are very complicated, others are simpler.

In this paper a framework for a complete model of the total deterioration process of reinforced concrete structures resulting from corrosion of the reinforcement is presented. The model includes chloride ingress, corrosion initiation, corrosion propagation, crack initiation, and crack opening models. The model is made as simple as possible, but may easily be extended to include space dependence, time dependence, and inhomogeneous and anisotropic materials.

It is necessary to make all models presented in this paper stochastic, since a number of uncertain parameters are included in the models. This includes the diffusion coefficient, the corrosion parameters, the rebar diameter, and the concrete cover etc., but also model uncertainties. The deterministic models presented are easily made stochastic by assuming that the involved parameters are stochastic variables or stochastic processes.

REFERENCES

[1] Ellingwood, B.R. Challenges to Condition Assessment of Aging Civil Infrastructure: Research and Implementation. Proceedings of ICOSSAR 2005, Rome, June 2005, cd-rom, Millpress, Rotterdam, 2005.

[2] Lundgren, K. Modelling the Effect of Corrosion on bond in Reinforced Concrete. Magazine of Concrete Research, Vol. 54 (3), 2002, pp.165-173.

[3] Maurel, O., Dekoster, M. and F. Buyle-Bodin (2005). Relation between Total Degradation of Steel Concrete Band and the Degree of Corrosion of RC Beams Experimental and Computational Studies. Computers and Concrete. Vol. 2, 1005, pp.1-18.

[4] Neville, A.M. Properties of Concrete. Fourth and Final Version, Prentice Hall, 2000.

[5] Nielsen, A. Hvid, grøn og sort rust (in Danish), Nr. 2, 1976.
[6] Frederiksen, J.M., Mejlbro, L. & Poulsen, E.. The HETEK model of Chloride Ingress into Concrete made simpler by Approximations. Testing and Modelling the Chloride Ingress into Concrete (eds. C. Andrade and J. Kropp), RILEM Proceedings, PRO 19, 2000, pp. 317-336.
[7] Mejlbro, L. The Complete Solution of Fick´s Second Law of Diffusion with time-dependent Diffusion Coefficient and Surface Concentration. Durability of Concrete in Saline Environment. CEMENTA, Danderyd, Sweden, 1996.
[8] Mejlbro, L. and Poulsen, E. (2000). On a model of Chloride Ingress into Concrete exposed to De-Icing Salt containing Chloride. Testing and Modelling the Chloride Ingress into Concrete (eds. C. Andrade and J. Kropp), RILEM Proceedings, PRO 19, 2000, pp. 337-354.
[9] Frederiksen, J.M. Chloride Threshold Values for Service Life Design. Testing and Modelling the Chloride Ingress into Concrete (eds. C. Andrade and J. Kropp), RILEM Proceedings, PRO 19, 2000, pp. 397-414.
[10] Thoft-Christensen, P. Modelling of the Deterioration of Reinforced Concrete Structures. Proceedings of IFIP Conference on Reliability and Optimization of Structural Systems, Ann Arbor, Michigan, 2000, pp.15-26.
[11] Jensen, O. M. Chloride Ingress in Cement Paste and Mortar Measured by Electron Micro Analysis. Technical Report Series R No.51, 1998. Department of Structural Engineering and Materials, the Technical University of Denmark.
[12] Jensen, O. M., Hansen P.F., Coats A.M. and Glasser, F.P.. Chloride Ingress in Cement and Mortar. Cement and Concrete Research, vol. 29, 1999, pp.1497-1504.
[13] Thoft-Christensen, P. Stochastic Modelling of the Diffusion Coefficient for Concrete. Proceedings of IFIP Conference on Reliability and Optimization of Structural Systems, Osaka, Japan, 2002, pp.151-159.
[14] Suda, K., S. Nagata & Y. Murayama. Development of Assessment System for Residual Life-Cycle Costs for Concrete Structures. Proceedings of Int. Workshop on “Life-Cycle Cost Analysis and Design of Civil Infrastructure Systems”, Yamaguchi University, Ube, Japan, September 2001, pp. 333-345.
[15] Collepardi, M., A. Marcialis & R. Turriziani. The Kinetics of Penetration of Chloride Ions into the Concrete (in Italian), Il Cemento, Vol. 67, N.4, 1270, pp. 157-164 .
[16] Luping, T. Chloride Transport in Concrete – Measurements and Prediction, Dissertation Chalmers University of Technology, Department of Building Materials, Publication P-96: 6, 1996.
[17] Jakobsen, U. et al. Determination of Water to Cement Ratio in Hardened Concrete by Optical Fluorescence Microscopy, ACI SP 191, 2000.
[18] Concrete-experts. Determination of w/c by fluorescence microscopy. http://www.concrete-experts.com/pages/wc.htm.
[19] Cappelen, J. 2002. Yerly Temperature, Precipitation, Hours of Bright Sunshine and Cloud Cover for Denmark as a whole; 1873-2001. Danish Meteorological Institute, Copenhagen, Technical Report 02-07.
[20] Thoft-Christensen, P. and Jensen, F.M. Revision of the Bridge Assessment Rules Based on Whole Life Performance: Concrete, Final Report, Highways Agency Contract DPU 9/3/44. CSRconsult ApS, December 1996.
[21] Liu, Y. and Weyers, R.E. Modelling of the Time to Corrosion Cracking in Chloride Contaminated Reinforced Concrete Structures. ACI Materials

Journal, Vol. 95, 1998, pp. 675-681.
[22] Andrade, C., Alonso, C. & Molina, F.J.. Cover Cracking as a Function of Bar Corrosion: Part 1-Experimental Test. Materials and Structures, Vol. 26, 1993, pp. 453-464.
[23] Thoft-Christensen, P. (2004). Modelling Corrosion Cracks. Proc. IFIP TC7 Conference, Sophia Antipolis, France, 2003. In J. Cagnol & J-P. Zolesio (editors), Information Processing: Recent Mathematical Advances in Optimization and Control. Mathematical Computational Sciences, Presses de l'Ecole des Mines de Paris, 2004, pp. 25-33.
[24] Thoft-Christensen, P., S. Svensson and H.L. Frandsen. 3-D Modelling of Corrosion Crack Opening. Proceedings of IFIP WG 7.5 Conference, Aalborg, Denmark, May 2005. In "Advances in Reliability and Optimization of Structural Systems" (eds. J.D. Sørensen and M. Frangopol), Taylor & Francis, 2006, pp.163-170.
[25] Thoft-Christensen, P. Proc. Int. Conf. on "Modelling and Optimization of Structures, Processes and Systems", ICMOSP 07, Durban, South Africa, January 22-24, 2007.
[26] Thoft-Christensen, P. Frandsen, H.I. & Svensson, S. Numerical Study of Corrosion crack Opening. Structure and Infrastructure Engineering, Vol. 4, 2008, pp.381-391.
[27] Thoft-Christensen, P. FEM Modelling of the Evolution of Corrosion Cracks in Reinforced Concrete Structures. Proc. IFIP WG7.5 Conference on "Optimization and Reliability of Structural Systems", Banff, Canada, Nov. 2003, September 25-27 2003, pp. 221-228.